Available online at www.sciencedirect.com
SCIENCE DIRECT®
ELSEVIER
Ultramicroscopy 101 (2004) 129–138
ultramicroscopy
www.elsevier.com/locate/ultramic

Normalizing projection images: a study of image normalizing procedures for single particle three-dimensional electron microscopy

C.O.S. Sorzano[a], L.G. de la Fraga[b], R. Clackdoyle[c], J.M. Carazo[a,*]

[a] *Biocomputing Unit, National Center of Biotechnology (CSIC), Campus Universidad Autónoma, 28049 Cantoblanco, Madrid, Spain*
[b] *Computer Science Section, Department of Electrical Engineering. CINVESTAV-IPN Av. Instituto Politécnico Nacional 2508, 07300 México DF, Mexico*
[c] *Medical Imaging Research Laboratory, Department of Radiology, Utah University, CAMT 729 Arapeen Drive, Salt Lake City, UT 84108-1218, USA*

Received 25 February 2003; received in revised form 8 April 2004; accepted 13 April 2004

Abstract

In the process of three-dimensional reconstruction of single particle biological macromolecules several hundreds, or thousands, of projection images are taken from tens or hundreds of independently digitized micrographs. These different micrographs show differences in the background grey level and particle contrast and, therefore, have to be normalized by scaling their pixel values before entering the reconstruction process. In this work several normalization procedures are studied using a statistical comparison framework. We finally show that the use of the different normalization methods affects the reconstruction quality, providing guidance on the choice of normalization procedures.
© 2004 Elsevier B.V. All rights reserved.

PACS: 87.59.−e; 87.59.Fm; 87.64.Dz

Keywords: Single particles; Electron microscopy; Image normalization; Image formation model; Computed tomography

1. Introduction

Structural biology aims at the acquisition and analysis of the three-dimensional structure of biological macromolecules. This information is essential to fully understand the molecular machinery that supports life. Experimentally, the structural information can be collected using different techniques such as X-ray crystallography [1], NMR [2] and electron microscopy (EM) either as electron crystallography [3], tomography [4] or single particle reconstruction [5–8].

Single particle reconstructions assume that all projection images come from a unique specimen.

*Corresponding author. Tel.: +34-1-5854543; fax: +34-1-5854506.
E-mail address: carazo@cnb.uam.es (J.M. Carazo).

0304-3991/$ - see front matter © 2004 Elsevier B.V. All rights reserved.
doi:10.1016/j.ultramic.2004.04.004

However, this is not exactly true since different projections are taken from different specimens which are supposed to be structurally identical up to a certain resolution. Three important issues have to be solved before entering the reconstruction process. First, one must be sure that all projections are from the desired specimen, avoiding projection images where the specimen was severely damaged or projections of other kinds of particles [9]. Second, a common geometrical framework (angular assignment and particle displacement) must be established for all projections such that every projection image represents a certain point of view of the same volume [10, Chapter 5]. Finally, the projection grey values must be coherent among projections. Usually this step is carried out by normalization of the image grey values [8].

A number of normalizing procedures have been proposed over the years. However, a detailed analysis of the properties, advantages and disadvantages of each one is lacking. This work explores and compares the different alternatives appearing in the literature.

The analysis will follow a two-step procedure. Firstly, the different normalizing procedures will be analyzed theoretically according to a given image model and then the analysis will be validated by experiment simulation. These simulations involve a 3D reconstruction step since it is at the stage of combining non-compatible projections where the effect of an improper normalization should appear more strongly.

2. Normalization procedures

In this section a theoretical analysis of the normalization step is performed. First of all, an image formation model is needed. Let $I_{\mathrm{id}}(x,y)$ be the ideal projection of the volume to be reconstructed along some direction. This ideal projection has exact density values since it is computed as the line integral along the volume density. At this point, we will follow a black-box system-theory approach, i.e., any transformation that our ideal image might suffer can be expanded in Taylor series. A first order approximation of the relationship between the measured image and the ideal image is given by

$$I(x,y) = A[I_{\mathrm{id}}(x,y) + n(x,y)] + B, \tag{1}$$

where $n(x,y)$ is a white Gaussian noise of zero mean and A and B define a linear transformation. It should be noticed that this simple model is able to account for the differences in contrast (through the A parameter) and background average values (through the B parameter) among the set of projections. It must also be pointed out that A and B need not be the same for all images coming from the same micrograph and that they are totally independent. It will be assumed that every projection image is affected by a particular linear transformation. Physical differences in the sample preparation, film development and digitization can be directly translated into differences in the A and B parameters. However, it is not our aim in this paper to point out the exact relationship between each physical process involved and the linear transformation coefficients.

Obviously, a more realistic image formation model should include the correlation between pixels introduced by the imaging devices. Assuming that the whole imaging system is shift invariant, a first order description of this correlation is provided by the linear-system theory. The output of the system is modeled by the convolution of the system impulse response (or Point Spread Function, PSF) with the ideal image

$$I(x,y) = A\{\mathrm{PSF} * [I_{\mathrm{id}}(x,y) + n_{\mathrm{b}}(x,y)] + n_{\mathrm{a}}(x,y)\} + B, \tag{2}$$

where $*$ represents the convolution operation, n_{b} the noise generated before applying the PSF (therefore, it is affected by the PSF) and n_{a} the noise generated after the application of the PSF (not affected by the PSF).

This simple linear model can handle the microscope aberrations usually modeled in Fourier space by the contrast transfer function (CTF) [10, Chapter 2], the low-pass filter usually introduced by the scanner or the CCD camera used to digitize the images, the band-pass filter sometimes used by EM practitioners, etc. through the identification of the proper PSF. The noise model is also general enough so as to distinguish between

noise affected by the PSF (correlated noise) and noise that is not affected (uncorrelated). In this way, different noise sources can be addressed with this model: noise due to the electron count statistics, noise because of the film grain, film development, quantization noise in the digitization, CCD electronic noise, etc. Furthermore, this noise model with two separate components has been found useful in the estimation of the CTF in micrographs [11]. Again, we would like to emphasize that our aim in this paper is not to derive specific impulse responses or noise models for all the image-acquisition steps involved but to provide a system theory approach to the topic.

The different normalizing methods take the measured image $I(x,y)$ and produce a normalized image $\hat{I}(x,y)$. The following five normalizing procedures, $N_i : i \in \{0,1,2,3,4\}$, have been studied in this work. They are defined as follows:

$$\hat{I}_0(x,y) = N_0[I(x,y)] = I(x,y),$$

$$\hat{I}_1(x,y) = N_1[I(x,y)] = \frac{I(x,y) - \text{avg}[\text{bg}(I)]}{\text{avg}[\text{bg}(I)]},$$

$$\hat{I}_2(x,y) = N_2[I(x,y)] = \frac{I(x,y) - \text{avg}(I)}{\sqrt{\text{var}(I)}},$$

$$\hat{I}_3(x,y) = N_3[I(x,y)] = \frac{I(x,y) - \text{avg}[\text{bg}(I)]}{\sqrt{\text{var}[\text{bg}(I)]}},$$

$$\hat{I}_4(x,y) = N_4[I(x,y)] = \frac{I(x,y) - \text{avg}[\text{bg}(I)]}{\text{avg}(I) - \text{avg}[\text{bg}(I)]}, \qquad (3)$$

where $\text{avg}(I)$ and $\text{var}(I)$ are the average and variance, respectively, of the set of density values of the image $I(x,y)$, and $\text{bg}(I)$ is the set of background density values of the image $I(x,y)$. In our implementation the background values are taken from those projection regions where there is no projection of the volume.

The procedure called N_0 corresponds to not taking any action at all and is included here for comparison purposes. The methods N_1 and N_2 correspond to the most widely used approaches in the field of three-dimensional electron microscopy [8,12–14]. The method N_3 has never been introduced formally before in EM single particle studies, although it can be easily proved that the normalization procedure used by Boisset et al. [15] is reduced to this procedure N_3 under the assumption of a Gaussian noise distribution. N_4 corresponds to a new method introduced in this work.

3. Results

This section starts with a theoretical study of the different normalization methods under study. First, the simplistic case in which no CTF is considered (Eq. (1)) is discussed (Section 3.1), followed by the more realistic case expressed by Eq. (2) (Section 3.2). Section 3.3 checks the assumption of a Gaussian noise distribution using experimental images acquired with a TEM. Finally, simulated data have been used in order to further validate the theoretical study carried out. The goal is to elucidate the effective accuracy and robustness of the different normalization procedures under common microscopy conditions: the variability of the linear transformation affecting each projection and changes in the CTF defocus. The simulation results are presented in Section 3.4.

3.1. Theoretical analysis considering a simple image formation model

At this point the statistical properties (average and variance) of the normalized images are studied. In order to present consistent information to the reconstruction algorithm, all projection images taken from a single specimen should have the same average (providing that all images are of the same size) while their variances may be different. If different projection images are subjected to different linear transformations and this effect is not removed by the normalization procedure, then the information provided to the 3D reconstruction algorithm would be inconsistent.

We start with the simple image formation model expressed by Eq. (1), and introduce this model into the normalization methods. Then, we get the set of expected values shown in Table 1. For instance, in this table it can be seen that the average value of

Table 1
Expected values of the mean and variance for the whole projection and its background using the different normalization procedures

Image	Model	Image average	Image variance	Background average	Background variance
Ideal projection	I_{id}	μ	σ^2	0	0
Projection with noise	$I_{id}+n$	μ	$\sigma^2+\sigma_n^2$	0	σ_n^2
Measured projection	$I=A(I_{id}+n)+B$	$A\mu+B$	$A^2(\sigma^2+\sigma_n^2)$	B	$A^2\sigma_n^2$
N_0	$\hat{I}_0=A(I_{id}+n)+B$	$A\mu+B$	$A^2(\sigma^2+\sigma_n^2)$	B	$A^2\sigma_n^2$
N_1	$\hat{I}_1=\frac{A(I_{id}+n)}{B}$	$\frac{A\mu}{B}$	$\frac{A^2(\sigma^2+\sigma_n^2)}{B^2}$	0	$\frac{A^2\sigma_n^2}{B^2}$
N_2	$\hat{I}_2=\frac{I_{id}+n-\mu}{\sqrt{\sigma^2+\sigma_n^2}}$	0	1	$\frac{-\mu}{\sqrt{\sigma^2+\sigma_n^2}}$	$\frac{\sigma_n^2}{\sigma^2+\sigma_n^2}$
N_3	$\hat{I}_3=\frac{I_{id}+n}{\sigma_n}$	$\frac{\mu}{\sigma_n}$	$\frac{\sigma^2+\sigma_n^2}{\sigma_n^2}$	0	1
N_4	$\hat{I}_4=\frac{I_{id}+n}{\mu}$	1	$\frac{\sigma^2+\sigma_n^2}{\mu^2}$	0	$\frac{\sigma_n^2}{\mu^2}$

Table 2
Expected values of the mean and variance for the whole projection and its background using the different normalization procedures

Image	Image average	Image variance	Background average	Background variance
N_0	$\mu_A\mu+\mu_B$	$(\mu_A^2+\sigma_A^2)(\sigma^2+\sigma_n^2)+\mu^2\sigma_A^2+\sigma_B^2$	μ_B	$(\mu_A^2+\sigma_A^2)\sigma_n^2+\sigma_B^2$
N_1	$\frac{\mu_A\mu}{\mu_B}+\frac{\mu_A\mu\sigma_B^2}{\mu_B^3}$	$\frac{(\mu_A^2+\sigma_A^2)(\sigma^2+\sigma_n^2)+\mu^2\sigma_A^2}{\mu_B^2}+\frac{\mu_A^2\mu^2\sigma_B^2}{\mu_B^4}$	0	$\frac{\mu_A^2\sigma_n^2}{\mu_B^2}$

the measured image is $A\mu+B$ while the average value in its background is only B.

It can be seen that most of the methods fixes two of the considered statistics to given values. For instance, the N_2 method sets the image average to 0 and the image variance to 1, while the N_3 method sets the background average to 0 and the background variance to 1. For each method, the sets of statistics that are not fixed (for instance, the background average and variance for method N_2) depend on the measured image features (the ideal image average and variance, and the variance of the added noise).

Any reminiscence of the linear transformation in the normalized images is understood as the inability of the normalization method to remove its effect. However, if the variances of the linear transformation parameters are small, i.e., if all projections are subjected to nearly the same linear transformation, then A and B are nearly constants and a dependence on A and B in the normalized images would not result in severe artifacts. In fact, if all ideal projections were transformed exactly in the same way, there would not be any need for normalization.

As is seen in Table 1, normalizations N_0 and N_1 are not able to remove the effect of the linear transformation. If it is assumed that all particles belonging to the same micrograph have suffered similar linear transformations, then the linear transformation parameters A and B of each projection must be similar to the ones in the rest of the micrograph. We model this fact by assuming that A and B are two Gaussian random variables with parameters μ_A, σ_A^2, and μ_B, σ_B^2, respectively. If the random nature of A and B is considered, then the statistics of the images normalized using the methods that are not able to remove the linear transformation, N_0 and N_1, must be changed to those shown in Table 2. In this table it can still be seen the dependency of the statistics of the normalized projections on the transformation parameters.

Let us analyze now the rationale of the methods that remove the dependence with the linear transformation. It should be noticed that the ideal projections share the same image average while their variance differs from one image to another. Furthermore, when white Gaussian noise is added to the perfect projections the background variance should be that of the added noise, i.e., some specified constant independent of the whole image variance. This is not the case of normalization N_2 where the image variances are all set to constant while it is the background noise power the one depending on the added noise and the ideal projection variance. However, as is shown in the simulation experiments, this effect does not substantially affect the reconstruction quality.

So far, it has been proved that N_3 and N_4 have good statistical properties consistent with what is expected from the ideal case. However, the following objection on N_4 can be stated. Electron microscopy images usually have very low signal-to-noise ratios and contrast-to-noise ratios [16]. This fact make the estimation of the difference between the image and the background sometimes be negative, although it should always be positive in the case of ideal projections with additive noise. This difference estimation is the denominator of the fraction involved in normalization N_4 and, thus, if it is negative the image contrast is reversed making the projection useless for 3D reconstruction.

An interesting point of normalizations N_3 and N_4 is that they allow the application of positivity constraints on the reconstructed volume [17] in the absence of CTF effects. The ideal volume, the one from which the ideal projections were taken, represents the mass density distribution in space, which is nonnegative. In this situation the projection of this ideal volume must also be nonnegative. After adding zero-mean noise the non-negativity of the projection is no longer true. However, the projection background must have a zero mean and the whole image a positive average. After linearly transforming each projection no statement on the projection average nor the background one can be done. Nevertheless, normalizations N_3 and N_4 take each measured projection back to a stage similar to that one before linearly transforming: the image average is positive while the background is zero-mean. At this stage it can be assured that the mass density originated from the ideal object must be positive in the normalized projection. In particular, when the ART reconstruction algorithm [18] is applied this fact imposes a nonlinear restriction on the reconstruction process which allows better reconstructions as is shown in the Section 3.4 and in [17]. Basically, after presenting each projection to the reconstruction algorithm, a new set of equations is imposed for those positions in the three-dimensional space with negative values. The new equations force the basis function combination at those points to be zero.

3.2. Theoretical analysis considering a more realistic image formation model

If the PSF is considered in the image formation model (see Eq. (2)), then the expected values of the average and the variance produced by each method change slightly to reflect the presence of the two different noises (one before the PSF, n_b, and another after the PSF, n_a) and the PSF itself. Both noises are supposed to be Gaussian with zero average. Plugging again the image formation model into the normalization procedures, the expected values in the whole image and the background can be computed. These values are shown in Table 3.

The analogy of the expected values with the case without considering PSF is obvious and, thus, the same conclusions can be drawn for the case with PSF. However, the average value of the PSF (which corresponds to the component of the Fourier transform of the PSF at frequency zero), in principle different for each image, modulates the average in the measured image and, therefore, the statistics of the normalized images. Different projection images may have different averages, even after normalization (see methods N_2 and N_3), if they undergo PSFs with different average. In this sense, it seems that N_4 is the best of the methods. However if the average of the PSF is null or very low, this method would not be applicable or would become highly unstable since the PSF average appears as a multiplicative factor in the denominator of the expression of the normalized image.

Table 3
Expected values of the mean and variance for the whole projection and its background using the different normalization procedures

Image	Model	Image average	Image variance	Background average	Background variance
Ideal projection	I_{id}	μ	σ^2	0	0
Measured projection	$I = A(\mathrm{PSF} * [I_{id} + n_b]) + n_a) + B$	$\overline{\mathrm{PSF}}A\mu + B$	$A^2(\sigma^2_{\mathrm{PSF}*I_{id}} + \sigma^2_{\mathrm{PSF}}\sigma^2_{nb} + \sigma^2_{na})$	B	$A^2(\sigma^2_{\mathrm{PSF}}\sigma^2_{nb} + \sigma^2_{na})$
N_0	$\hat{I}_0 = A(\mathrm{PSF} * [I_{id} + n_b) + n_a] + B$	$\overline{\mathrm{PSF}}A\mu + B$	$A^2(\sigma^2_{\mathrm{PSF}*I_{id}} + \sigma^2_{\mathrm{PSF}}\sigma^2_{nb} + \sigma^2_{na})$	B	$A^2(\sigma^2_{\mathrm{PSF}}\sigma^2_{nb} + \sigma^2_{na})$
N_1	$\hat{I}_1 = \dfrac{A(\mathrm{PSF} * [I_{id} + n_b] + n_a)}{B}$	$\dfrac{\overline{\mathrm{PSF}}A\mu}{B}$	$\dfrac{A^2(\sigma^2_{\mathrm{PSF}*I_{id}} + \sigma^2_{\mathrm{PSF}}\sigma^2_{nb} + \sigma^2_{na})}{B^2}$	0	$\dfrac{A^2(\sigma^2_{\mathrm{PSF}}\sigma^2_{nb} + \sigma^2_{na})}{B^2}$
N_2	$\hat{I}_2 = \dfrac{\mathrm{PSF} * [I_{id} + n_b] + n_a - \overline{\mathrm{PSF}}\mu}{\sqrt{\sigma^2_{\mathrm{PSF}*I_{id}} + \sigma^2_{\mathrm{PSF}}\sigma^2_{nb} + \sigma^2_{na}}}$	0	1	$\dfrac{-\overline{\mathrm{PSF}}\mu}{\sqrt{\sigma^2_{\mathrm{PSF}*I_{id}} + \sigma^2_{\mathrm{PSF}}\sigma^2_{nb} + \sigma^2_{na}}}$	$\dfrac{\sigma^2_{\mathrm{PSF}}\sigma^2_{nb} + \sigma^2_{na}}{\sigma^2_{\mathrm{PSF}*I_{id}} + \sigma^2_{\mathrm{PSF}}\sigma^2_{nb} + \sigma^2_{na}}$
N_3	$\hat{I}_3 = \dfrac{\mathrm{PSF} * [I_{id} + n_b] + n_a}{\sqrt{\sigma^2_{\mathrm{PSF}}\sigma^2_{nb} + \sigma^2_{na}}}$	$\dfrac{\overline{\mathrm{PSF}}\mu}{\sqrt{\sigma^2_{\mathrm{PSF}}\sigma^2_{nb} + \sigma^2_{na}}}$	$\dfrac{\sigma^2_{\mathrm{PSF}*I_{id}} + \sigma^2_{\mathrm{PSF}}\sigma^2_{nb} + \sigma^2_{na}}{\sigma^2_{\mathrm{PSF}}\sigma^2_{nb} + \sigma^2_{na}}$	0	1
N_4	$\hat{I}_4 = \dfrac{\mathrm{PSF} * [I_{id} + n_b] + n_a}{\overline{\mathrm{PSF}}\mu}$	1	$\dfrac{\sigma^2_{\mathrm{PSF}*I_{id}} + \sigma^2_{\mathrm{PSF}}\sigma^2_{nb} + \sigma^2_{na}}{\overline{\mathrm{PSF}}^2\mu^2}$	0	$\dfrac{\sigma^2_{\mathrm{PSF}}\sigma^2_{nb} + \sigma^2_{na}}{\overline{\mathrm{PSF}}^2\mu^2}$

σ^2_{PSF} is the power of the microscope impulse response while $\sigma^2_{\mathrm{PSF}*I_{id}}$ is the power of the ideal projection convolved with the PSF. $\overline{\mathrm{PSF}}$ is the average value of the PSF.

On the other hand, methods N_2 and N_3 rely on the estimation of the white noise power measured at the image background. However, the white noise is now affected by the PSF and, thus, the output noise power is modified by the shape of the PSF as can be seen in the corresponding image or background averages in Table 3. This effect can be easily corrected just by a multiplicative factor depending on the area below the square of the PSF providing a good estimate of the PSF is available. However, as will be shown by computer simulations, even if no correction for the noise power is applied, these two methods provide reasonably good results.

3.3. Analysis of experimental micrographs

To determine the distribution of noise and the variability of linear transformation parameters A and B that occur in practice, we studied the set of experimental cryo-micrographs used by Barcena et al. [14] in their study of the DnaBC complex. We started with the assumption that the background noise was Gaussian.

Given a projection image of size 100×100, all pixels outside a circle centered in the image, of radius 38 were considered to belong to the background. The normality assumption on the background noise was checked using the non-parametric Kolmogorov–Smirnov test [19, Chapter 14]. The hypothesis that the background noise was normal was accepted with a confidence of 99%, for the 93% of 8046 analyzed DnaB-C projections. This figure suggests that the measured background noise is effectively Gaussian.

We also estimated the distribution of the linear transformation parameters, A and B. The background noise was assumed to be the linear transformation of a Gaussian zero-mean random process with unit standard deviation ($n_{\mathrm{measured}} = An_{\mathrm{ideal}} + B$). The variance of the bias, B, was found to be $\sigma^2_B = 3.7\%$ of its average while the variance of the multiplicative factor, A, was about $\sigma^2_A = 3.9\%$.

As for the image averages it turned out that the 34% of the considered projections showed a background average slightly greater than the whole image average.

3.4. Results of computer simulations

In order to establish the robustness and accuracy of the normalization procedures, simulated experiments were performed. Two different situations were explored: linear transformation changes and CTF defocus changes. A phantom volume of the bacteriorhodopsin [20] was created at a resolution of 3.5 Å. one-thousand random and evenly distributed projections were taken from this volume, and noise was added up to a signal-to-noise ratio of 0.3. Then the projections were transformed according to each of the studied situations: changes in the linear transformation and changes in the CTF defocus (the details for these transformations are described below.) Alignment and angular noise was also simulated: a random shift distributed as $N(0,2)$ pixels was applied in the X- and Y-directions, and a random number $N(0,5)$ degrees was added to the Euler angles. These projections were normalized using each of the considered procedures and then combined into a single 3D reconstruction using a linear reconstruction algorithm (ART + blobs [18]). Finally, the reconstruction quality was assessed using the resolution measure given when the Fourier shell correlation (FSC) [21] falls below 0.5. It should be noticed that the FSC is a similarity measure independent of the exact voxel densities.

For the study of the normalizing accuracy and robustness in the case of changes in the linear transformation, the A and B of Eq. (1) were normally distributed with variances of the 5% of their respective nominal values. The nominal values were chosen in accordance to those encountered in the statistical analysis performed on the experimental images that we introduced in the preceding section. Particularly, the nominal value for A was 139 and for B 547. Thirty experiments were carried out for each normalization procedure changing the noise realization and angular distribution in each one. After analyzing the FSC it was found that near all normalizing procedures yielded practically similar performance (see Table 4 and Fig. 1). As N_3 allows positivity constraints to be imposed on the reconstructed volume, the comparison has been extended to the case of normalizing the projection images using N_3 and adding positivity constraints during the reconstruction process (marked as $N_3 + pos$). A statistical comparison of the average resolution achieved by each method shows that the hypothesis that N_1, N_2, N_3 and N_4 have the same performance can be accepted with a confidence greater than 95%. In the same way, N_0 and $N_3 + pos$ show average resolutions that are different to the ones of N_1, N_2, N_3 and N_4 with a confidence greater than 95%.

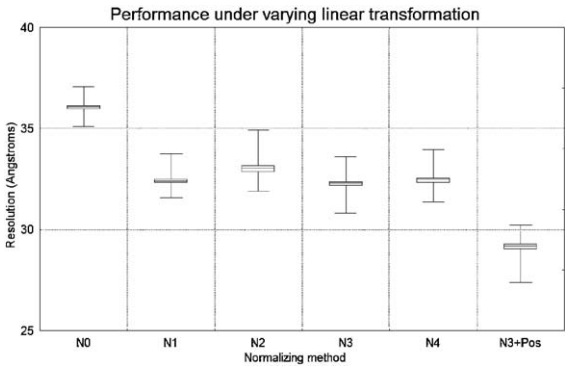

Fig. 1. Resolution in angstroms achieved by the 3D reconstructions when the computer-simulated input projections were normalized by each of the methods considered in this work and the input projections vary in the linear transformation suffered. The box represents the average value plus/minus a standard deviation, while the whiskers represent the maximum and minimum value.

Table 4
Resolution in angstroms achieved by the 3D reconstructions when the computer-simulated input projections were normalized by each of the methods considered in this work and the input projections vary in the linear transformation suffered

N_0	N_1	N_2	N_3	N_4	$N_3 + pos$
36.05 ± 0.35	32.20 ± 0.7	32.90 ± 0.7	32.20 ± 0.7	32.55 ± 0.7	29.05 ± 0.7

EM practitioners sometimes band-pass filter experimental images in order to get rid of artifacts caused by the different signal modulations encountered [8]. This case can be easily modeled in our formulation by introducing the appropriate PSF in the image formation model (see Section 3.2). In order to test the stability of the normalizing procedures in this situation, the previous experiment (random variation of the linear transformation) was repeated when the input images were high-pass filtered with a cutoff resolution of 117 Å. The resolution achieved by each of the methods was not significantly different (with a confidence of 95%) from those obtained when the images were not filtered except for N_0 whose resolution was 37.91 ± 0.5.

For the study of robustness and accuracy under changes of the CTF defocus, we randomly changed this parameter within a 10% of its nominal value (2.75 μm). The formula used for the CTF implementation is the one given by Zhou et al. [22] and the plot of the nominal CTF is represented in Fig. 2. The phantom, collection geometry and noise applied to the angles and shifts as well as to the pixel values remain the same as in the previous experiment. This experiment is intended to measure the robustness of the proposed normalizing methods with respect to changes in the CTF profile. The results obtained are summarized in Table 5 and Fig. 3. It should be noticed that in this experiment algorithms N_1 and N_4 become highly unstable and thus only a few measures (around 8) are reliably computed from the repetition series performed. This instability is also the reason why $N_4 + pos$ has not been investigated since in real-life experiments it is not always guaranteed that N_4 is applicable. A statistical comparison of the average resolution achieved by each method show that N_3 and N_4 show no significantly different performance with a confidence greater than 95%, whereas the rest of methods have different means with a confidence greater than 95%.

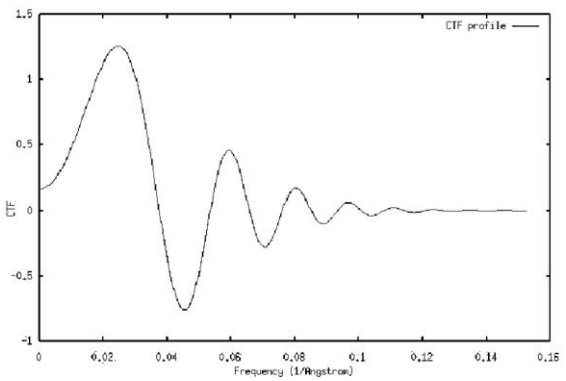

Fig. 2. Radial plot of the CTF used in the simulations.

Table 5
Resolution in angstroms achieved by the 3D reconstructions when the computer-simulated input projections were normalized by each of the methods considered in this work and the input projections vary in the defocus of the CTF applied

N_0	N_1	N_2	N_3	N_4	$N_3 + pos$
50.8 ± 9.5	59.8 ± 9.4	44.1 ± 6.3	47.2 ± 5.6	47.6 ± 5.6	37.1 ± 6.0

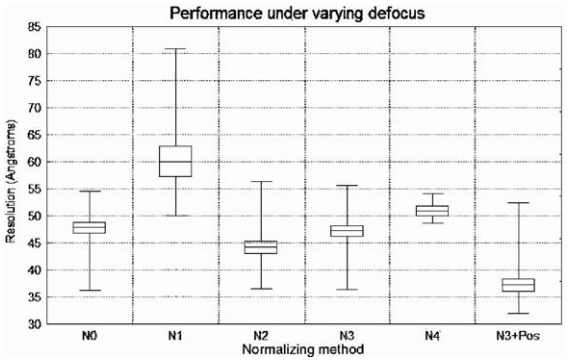

Fig. 3. Resolution in angstroms achieved by the 3D reconstructions when the computer-simulated input projections were normalized by each of the methods considered in this work and the input projections vary in the defocus of the CTF applied. The box represents the average value plus/minus a standard deviation, while the whiskers represent the maximum and minimum value.

4. Discussion

Normalization is usually performed as a step that brings all projections involved in a 3D reconstruction to a common numerical framework. In this way, the numerical values registered in the images are compatible with the existence of a volume that generated the projections. A failure

to meet this situation, i.e., the projection values are incompatible with the existence of a volume, would cause a deterioration of the reconstruction quality. In this work a theoretical study of the statistical properties of each normalization procedure has been carried out and computational experiments in order to compare the different normalizing methods have been run. The simulation experiments included the reconstruction step, which in this case was performed using the method known as ART + blobs [18].

The reconstruction resolution has been selected as a figure of merit reporting on the deterioration of the reconstruction. It must be noticed that this figure of merit is independent of the density values of the reconstruction. This makes a fair comparison among methods since in real-life reconstructions the exact density values of the volume to reconstruct is unknown and only relative variations are informative.

From the theoretical analysis it is clear that not all normalizing methods are valid in the sense that some of them do not remove the effect of the linear transformation (responsible for the changes in contrast and background average) on the collected projections. Warnings have been raised on the theoretical instability of N_4 and the inaccuracy of N_1, which indeed appear in the numerical simulations.

The experiment simulating the randomness of the linear transformation shows that most of the correcting methods behave similarly (in terms of resolution achieved). No significant resolution improvement has been obtained in this case by applying positivity constraints. The similar performance of the normalizing algorithms in these experiments seems to indicate that most of the normalizing methods commonly used in electron microscopy behave robustly as long as the variation in contrast and background level among projections is within certain limits (in the simulated case 5% of its nominal value).

However, the experiment changing the CTF defocus (a 10% of its nominal value) poses a more challenging problem to the normalizing process and the results of the normalizing algorithms are clearly different. A difference in resolution as high as 22 Å has been achieved in the experiment done by selecting a more suitable normalizing method. And this difference in resolution can be significantly increased if positivity constraints can be applied. Actually, they can only be applied if N_3 or N_4 are used, and the instability of N_4 plays against it when performing reconstructions with experimental data. Methods in general become more unstable as is shown by the increase in the variance of the resolution achieved. Methods N_1 and N_4 became highly unstable and many of the reconstructions performed with projections normalized by these methods showed high density artifacts spuriously distributed.

Methods N_2 and N_3 have shown to be robust and to provide reasonably good results in the two experiments carried out. Furthermore, N_3 is the only stable method among the studied ones allowing imposition of positivity constraints on the reconstructed volume. This constraint has proved to provide extra information especially useful in the case of the CTF change, even if the CTF phase is not corrected. The experiments carried out use a random evenly distributed set of projections, but our experience tells us that if the collection geometry leaves uncovered regions in Fourier space, then the positivity constraint constitutes a powerful tool to partially recover information in the missing region [17].

5. Conclusions

In this paper we have explored the theoretical and practical implications of different normalizing methods. We have theoretically shown that assuming that different projections have undergone different linear transformations resulting in variations among image contrast and background level, then not all normalizing procedures are able to remove the effect of the transformation. However, a study of the actual changes in cryomicrographs have shown that these differences are small, and in this way, the errors introduced in the 3D reconstruction are not significant. A more complicated problem is faced when the CTF defocus changes. In this case, a poor selection of the normalizing procedure can account for a significant deterioration of the reconstruction as

measured by the reconstruction resolution. Additionally, depending on the normalization selected we may impose positivity constraints on the reconstructed volume. This constraint has been shown to be especially useful in the case of changing the CTF defocus. We recommend using normalization method N_3 with the reconstruction algorithm ART + blobs. Of the choices studied, this method seems particularly effective in the presence of a slowly varying CTF and it allows the application of positivity constraints. The uncertainty about the exact area under the square of the CTF curve seems not to be a problem for the use of N_3.

Acknowledgements

Partial support is acknowledged to the "Comisión Interministerial de Ciencia y Tecnologıa" of Spain through project BIO98-0761, BIO2001-1237 and TIC990361 and to the NIH through grants HL740472 and HL67465-01.

The authors would like to thank Dr. Radermacher and Dr. Marabini for many fruitful discussions and good suggestions about the manuscript.

References

[1] J. Drenth, Principles of Protein X-ray Crystallography, Springer, New York, 1984.
[2] J. Jonas, High-resolution nuclear magnetic resonance studies of proteins, Biochim. Biophys. Acta 1595 (2002) 145.
[3] M.J. Ellis, H. Hebert, Structure analysis of soluble proteins using electron crystallography, Micron 32 (2001) 541.
[4] J.Böhm, A.S. Frangakis, R. Hegerl, S. Nickell, D. Typke, W. Baumeister, Toward detecting and identifying macromolecules in a cellular context: template matching applied to electron tomograms, Proc. Natl. Acad. Sci. USA 97 (2000) 14245.
[5] M. van Heel, B. Gowen, R. Matadeen, Single-Particle electron cryo-microscopy: towards atomic resolution, Q. Rev. Biophys. 33 (2000) 307.
[6] W. Kuhlbrandt, K.A. Williams, Analysis of macromolecular structure and dynamics by electron cryo-microscopy, Curr. Opin. Struct. Biol. 3 (1999) 537.
[7] Y. Tao, W. Zhang, Recent development in cryo-electrom microscopy reconstruction of single particles, Curr. Opin. Struct. Biol. 10 (2000) 616.
[8] J. Ruprecht, J. Nield, Determining the structure of biological macromolecules by transmission electron microscopy, single particle analysis and 3D reconstruction, Progr. Biophys. Mol. Biol. 75 (2001) 121.
[9] A. Pascual-Montano, L.E. Donate, M. Valle, M. Bárcena, R.D. Pascual-Marqui, J.M. Carazo, A novel neural network technique for analysis and classification of EM single-particle images, J. Struct. Biol. 133 (2001) 233.
[10] J. Frank, Three Dimensional Electron Microscopy of Macromolecular Assemblies, Academic Press, San Diego, CA, 1996.
[11] J.A. Velázquez-Muriel, C.O.S. Sorzano, J.J. Fernández, J.M. Carazo, A method for estimating the CTF in electron microscopy based on ARMA models and parameter adjusting, Ultramicroscopy 96 (2003) 17.
[12] M. Schatz, E.V. Orlova, P. Dube, K. Braig, M. van Heel, Structure of *lumbricus terrestris* hemoglobin at 30 Å resolution determined using angular reconstitution, J. Struct. Biol. 114 (1995) 28.
[13] A.M. Roseman, S. Chen, H. Write, K. Braig, H.R. Saibil, The chaperonin ATPase cycle: mechanism of allosteric switching and movements of substrate-binding domains in GroEL, Cell 87 (1996) 241.
[14] M. Bárcena, L.E. Donate, T. Ruiz, N. Dixon, M. Radermacher, J.M. Carazo, The DnaB-DnaC complex: a structure based on interactions among assymetric dimers, EMBO J. 20 (2001) 1462.
[15] N. Boisset, P. Penczek, F. Pochon, J. Frank, J. Lamy, Three-dimensional architecture of human α2-macroglobulin transformed with methylamine, J. Mol. Biol. 232 (1993) 522.
[16] Y. Sun, D. Parker, Small vessel enhancement in MRA images using local maximum mean processing, IEEE Trans. Image Process. 10 (2001) 1687.
[17] C.O.S. Sorzano, R. Marabini, G.T. Herman, J.M. Carazo, Volumetric constraints in 3D tomography applied to electron microscopy, in: Proceedings of the First International Symposium on Biomedical Imaging, Washington, USA, 2002, pp. 641.
[18] R. Marabini, G.T. Herman, J.M. Carazo, 3D reconstruction in electron microscopy using ART with smooth spherically symmetric volume elements (blobs), Ultramicroscopy 72 (1998) 53.
[19] W. Press, S.A. Teukolsky, W.T. Vetterling, B.P. Flannery, Numerical recipes in C, 2nd Edition, Cambridge University Press, Cambridge, 1992.
[20] T.A. Ceska, R. Henderson, J.M. Baldwin, F. Zemlin, E. Beckmann, K. Downing, An atomic model for the structure of bacteriorhodopsin, a seven-helix membrane protein, Acta Physiol. Scand. Suppl. 607 (1992) 31.
[21] M. van Heel, Similarity measures between images, Ultramicroscopy 21 (1987) 95.
[22] Z.H. Zhou, S. Hardt, B. Wang, M.B. Sherman, J. Jakana, W. Chiu, CTF determination of images of ice-embedded single particles using a graphics interface, J. Struct. Biol. 116 (1996) 216.